THE JOURNAL OF PHYSICAL CHEMISTRY B
A JOURNAL OF THE AMERICAN CHEMICAL SOCIETY

pubs.acs.org/JPCB

Article

Behavior of Long-Chain Hydrocarbons at High Pressures and Temperatures

Abhisek Basu,* Mainak Mookherjee, Ericka McMahan, Bianca Haberl, and Reinhard Boehler

Cite This: J. Phys. Chem. B 2022, 126, 2530−2537

Read Online

ACCESS | Metrics & More | Article Recommendations | Supporting Information

ABSTRACT: Although long-chain aliphatic hydrocarbons are documented in meteorites, their origin is poorly understood. A key question is whether they are pristine or a byproduct of terrestrial alteration? To understand if these long-chain hydrocarbons are indigenous, it will be important to explore their thermodynamic and mechanical stability at conditions experienced by extraterrestrial objects during atmospheric entry and passage. Extreme pressures and temperatures experienced by meteorites are likely to alter the molecular organization of these long-chain hydrocarbons. These structural changes associated with extreme conditions are often documented via laboratory-based Raman spectroscopic measurements. So far, Raman spectroscopic measurements have investigated the effect of static compression on the aliphatic hydrocarbons. The effect of temperature on the structural changes remains poorly explored. To bridge this gap, in this study, we have explored the behavior of two aliphatic hydrocarbons at simultaneously high pressures and temperatures. We have used a resistively heated diamond anvil cell. On compression to moderate pressures, the appearance of new vibrational modes in the low-energy region confirms prior studies and is related to the bending of the linear chains. Upon heating to ∼220 °C, we note that the new low-energy mode undergoes softening. The mode softening is likely due to the combination of unbending of the alkane chain and mode anharmonicity.

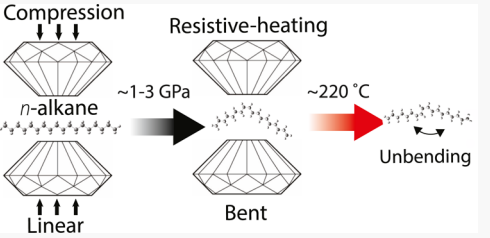

1. INTRODUCTION

Earth receives about 10^5-10^6 kg/day of extraterrestrial material in the form of interplanetary dust particles (IDPs), micrometeorites (MMs), and meteorites.[1] A particular group of meteorites is carbonaceous chondrites (CCs), a primordial class of chondritic meteorites, which contain a record of the evolution of the solar system and pre-solar information derived from asteroids.[2] This type of chondrite generally contains a carbon-rich matrix and is composed primarily of clay minerals, oxides, and organic matter.[3,4] However, CCs are known to undergo aqueous and chemical alterations in the parent body and experience a wide range of pressure and temperature during the atmospheric entry and passage and a variety of terrestrial contamination. As a result, while the organic matter in CCs has been extensively explored, its origin is often debated.[5−7] Similarly, MMs and IDPs are a host of several kinds of organic materials like aliphatic and polycyclic aromatic hydrocarbons, ketones, and amino acids.[8−12] Unlike CCs, the IDPs and MMs are the most primitive unaltered extraterrestrial materials available since they have escaped thermal and aqueous processing in their parent body which may have modified the mineralogy and constituents of primitive meteorites.[11]

Theoretical models and observations have suggested that depending on weight, density, and size, the peak surface temperature experienced by extraterrestrial objects during the atmospheric entry and passage is likely to be between 400 and 1700 °C,[13−18] though the peak interior temperatures experienced are reported to be lower.[19] The three families of organic matter found in IDPs and MMs—polycyclic aromatic hydrocarbons, ketones, and amino acids—have sublimation temperatures between 200 and 500 °C. For example, coronene sublimes at 525 °C, 2-pentadecanone at 293 °C, and amino acids at 170 °C.[20] Similarly, aliphatic hydrocarbons found in several meteorites including Orgueil (CI1), Alais (CI1), Tonk (CI1), Ivuna (CI1), and Murray (CM2) exhibit thermal stability within temperatures of 200−1200 °C. Previous studies have revealed that over geological time scales, liquid hydrocarbons progressively decompose to lighter hydrocarbons and ultimately to methane in the temperature region of 150−200 °C.[21−23] Solid alkanes like octadecane and nonadecane found in the Paris meteorite[4] undergo decomposition to diamond agglomerates and hydrogen at temperatures of more than 2700 °C and pressures in between 10 and 20 GPa.[24] Recent studies on heavier alkanes have revealed compression-induced bending of linear alkane chains, which led to the speculation of dissociation of the chains at the low-energy bent region if sufficient thermal energy is provided.[25,26] However, the actual dissociation process is not well understood and will likely depend on the actual pressure (P)−temperature (T) path

Received: December 22, 2021
Revised: February 21, 2022
Published: March 25, 2022

https://doi.org/10.1021/acs.jpcb.1c10786
J. Phys. Chem. B 2022, 126, 2530−2537

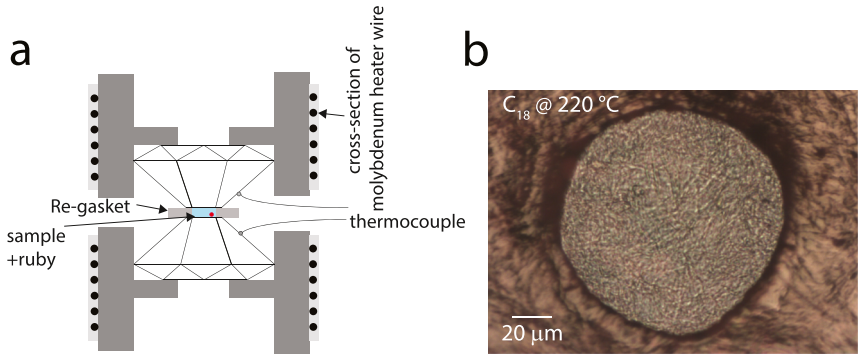

Figure 1. (a) Schematic diagram showing the internal heating mechanism of the HDAC. Molybdenum wires are coiled around the tungsten carbide seats, which indirectly heats the sample chamber through the anvils. Two thermocouple wires are placed close to the diamond anvils for accurate determination of temperature. (b) Image of the sample chamber, showing the sample C_{18} at 220 °C.

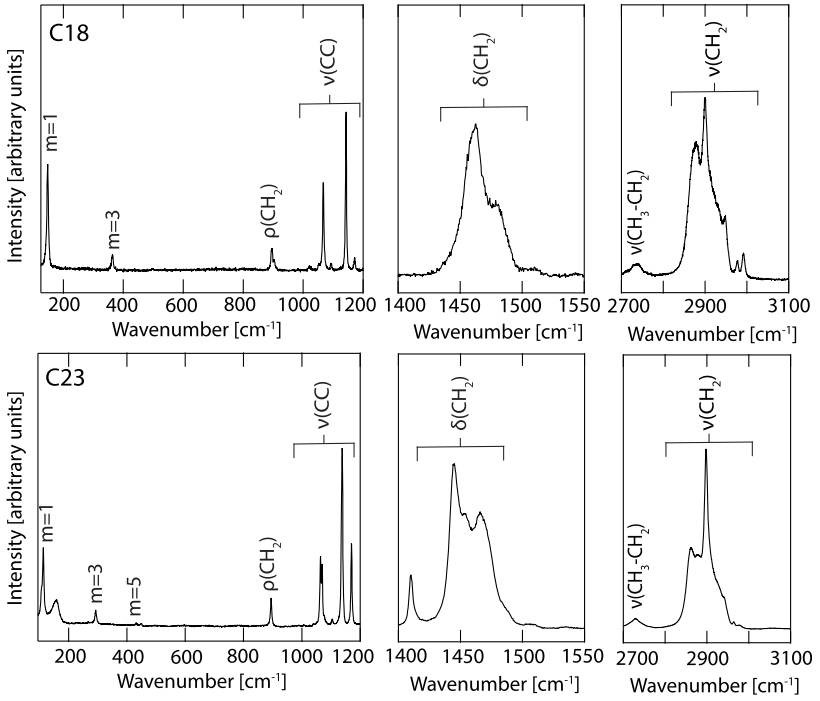

Figure 2. Raman spectrum of C_{18} and C_{23}. The fundament LAM is indicated by $m = 1$ and successive overtones by higher numbers. The C−C stretching mode is indicated by ν(CC), H−C−H rocking mode by $\rho(CH_2)$, H−C−H bending modes by $\delta(CH_2)$, and C−H stretching modes by $\nu(CH_2)$.

followed. Furthermore, the behavior of the long-chain aliphatic hydrocarbon at moderate temperatures and pressures remains relatively unknown.

Therefore, it will be important to understand the behavior of the aliphatic hydrocarbons at relatively low temperatures of up to 200 °C, mimicking the conditions in the interiors of the meteorites during entry. To address these questions, here we explore the pressure−temperature response of two aliphatic hydrocarbons—octadecane and tricosane. To enable insights into behaviors within the interior of extraterrestrial objects, a low $P-T$ regime up to ∼4.5 GPa and 220 °C was selected for this study. This allows us to model the behavior of aliphatic alkanes found in extraterrestrial objects.

2. METHOD

2.1. Aliphatic Hydrocarbon Samples. We have obtained the crystalline linear chain saturated aliphatic hydrocarbons (C_nH_{2n+2})—octadecane (n = 18, C_{18}) and tricosane (n = 23, C_{23}), samples from Alfa Aesar with >99% purity. Due to the low melting point (28 °C) of the C_{18} sample, we ensured that during the loading, it was not inadvertently exposed to temperatures above its melting point. The room temperature was maintained at 22 °C. We have collected the Raman spectra of the samples at ambient and elevated pressures and temperatures using a Horiba Jobin Yvon LabRAM Evolution Raman spectrometer located at the Earth Materials Laboratory, Department of Earth, Ocean, & Atmospheric Science, Florida State University. We used a frequency-doubled solid-state Nd:YAG laser with a 532 nm wavelength with a maximum power of 300 mW at the source. We collected the spectra using a 1800 L/mm grating, setting the resolution at 2 cm^{-1}. We focused the laser beam inside the diamond anvil cell sample chamber using a 50× infinity-corrected long working distance objective. To avoid the sample modification due to heating from the Nd:YAG laser, we measured the effects of laser at various power according to a previous study.[27]

https://doi.org/10.1021/acs.jpcb.1c10786
J. Phys. Chem. B 2022, 126, 2530−2537

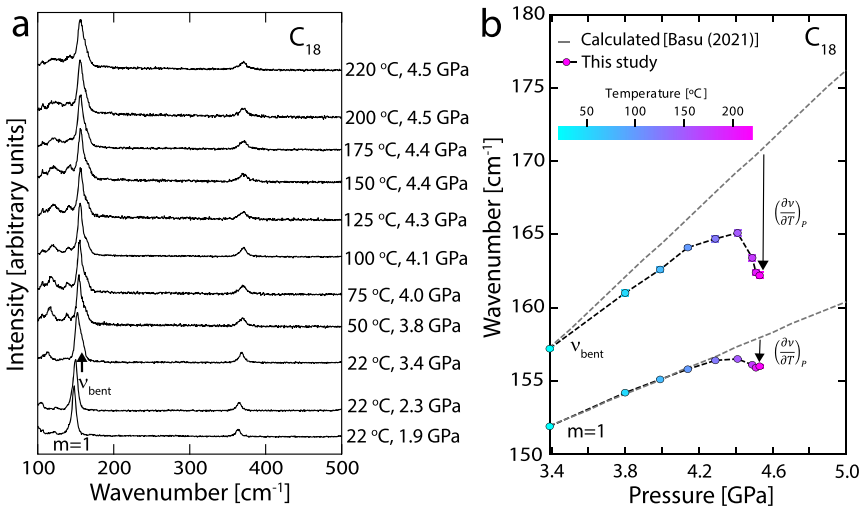

Figure 3. (a) Stacked Raman spectra of C_{18} in the low-energy region between 100 and 500 cm^{-1}. The temperature, applied through the resistive heating in an HDAC, is shown along with the observed pressures. The fundamental LAM (m = 1) and the new bent mode (ν_{bent}) are indicated. (b) Plot of the fundamental LAM (m = 1) and ν_{bent} mode of C_{18} as a function of pressure is shown. The temperature is shown as a color contour. The color scale is shown in the inset, as a reference, with cyan color indicative of lower temperatures and magenta indicative of higher temperatures. The dashed line represents the pressure dependence of the ν_{bent} mode at room-temperature compression, where the $(\partial\nu/\partial P)_{22\ °C}$ is obtained from previous estimates,[26] and ν_0 is obtained from this study. The $(\partial\nu/\partial T)_P$indicates the difference in the mode frequency between the static room temperature[26] and the HDAC high temperature (this study) measurements at a constant pressure. Please refer to the results section which elaborates further.

2.2. External Resistive Heating. To understand the effects of moderate temperatures up to ∼200 °C on the samples, we loaded the C_{18} and C_{23} in separate runs in a hydrothermal diamond anvil cell (HDAC).[27−29] The HDACs were equipped with a pair of low fluorescence diamonds with culet size ∼500 μm mounted on a tungsten carbide (WC) seat. We preindented a rhenium foil of 150 μm thickness to 50 μm and drilled a sample chamber of 150 μm diameter using the Almax-Boehler μ-driller. As the samples have high compressibility,[30] we loaded them without a pressure medium. We used molybdenum wire coiled around the seats to heat the samples (Figure 1). We used an integrated power controller from PES Enterprise to program the power delivered to the upper and lower heating coils attached to the WC seats. To measure the temperature, we placed two K-type thermocouples close to the sample chamber attached to the diamond anvil facets. We noted a temperature difference of ∼ ±1 °C between the upper and lower thermocouple during the heating and cooling cycle. We heated the sample to the maximum temperature of 220 °C. To measure the pressure, we loaded a few micron grains of ruby and determined pressure using the ruby fluorescence method.[31]

3. RESULTS

3.1. Raman Spectra of C_{18} and C_{23} under Ambient Conditions. The ambient condition Raman spectra of C_{18} and C_{23} can be characterized by vibrations related to the (1) oscillation of the carbon atoms in the hydrocarbon chain simulating an accordion motion known as longitudinal accordion mode (LAM), (2) C−C stretching (ν) mode, (3) H−C−H twisting (τ) mode, (4) H−C−H bending (δ) modes, and (5) C−H stretching (ν) modes (Figure 2).[25,26] The observed modes in the wavenumber region till 600 cm^{-1} are due to LAM's. The fundamental LAM, that is, m = 1, is the lowest energy mode and observed at wavenumber ∼131 cm^{-1} for C_{18} and ∼103 cm^{-1} for C_{23}. The LAM frequency is given by

$$\nu^2 = \left(\frac{2C}{M}\right)(1 - \cos kl)$$

where C is the force constant, M is the reduced mass of atoms, $k = m\pi/l$ is the wavevector, and m = 0,1,2,3,...,n.[25] We find an approximately inverse relationship between the hydrocarbon chain length, that is, the number of atoms in an alkane chain (n) and the fundamental LAM frequency.[25,26] The LAM overtones, that is, m = 3, 5, were observed at higher frequencies where the mode intensity reduced significantly such that overtones beyond m = 5 were not discernible. The modes in the wavenumber region between 800 and 1250 cm^{-1} are characterized by symmetric and asymmetric stretching of C−C atom pairs and rocking motions of the H−C−H cluster of atoms. In general, the C−C stretching modes for the alkanes are observed between 950 and 1150 cm^{-1}, the C═C stretching modes for alkenes around 1450−1750 cm^{-1}, and the C≡C stretching modes for the alkynes in the region around 2100−2250 cm^{-1}, approximately.[25,26,32] The wavenumber region between 1400 and 1600 cm^{-1} is characterized by bending or scissoring vibrations of the H−C−H clusters, and the region between 2600 and 3000 cm^{-1} is characterized by C−H stretching vibrations.

3.2. External Resistive Heating of C_{18} and C_{23}. In a series of recent static high-pressure Raman spectroscopic studies on C_{18} and C_{23} conducted at room temperatures, the appearance of multiple new low wavenumber modes close to the fundamental LAM in the pressure regime of 0.3−3 GPa[25,26] was observed. Complementary *first-principles* simulations on linear and bent long-chain alkanes provided valuable insights into pressure-induced low-energy modes.[25,26] The high-pressure experimental study and complementary Raman spectra based on *first-principles* provided clues to how linear chains, C_{18} and C_{23}, transformed to a bent geometry at the

https://doi.org/10.1021/acs.jpcb.1c10786
J. Phys. Chem. B 2022, 126, 2530−2537

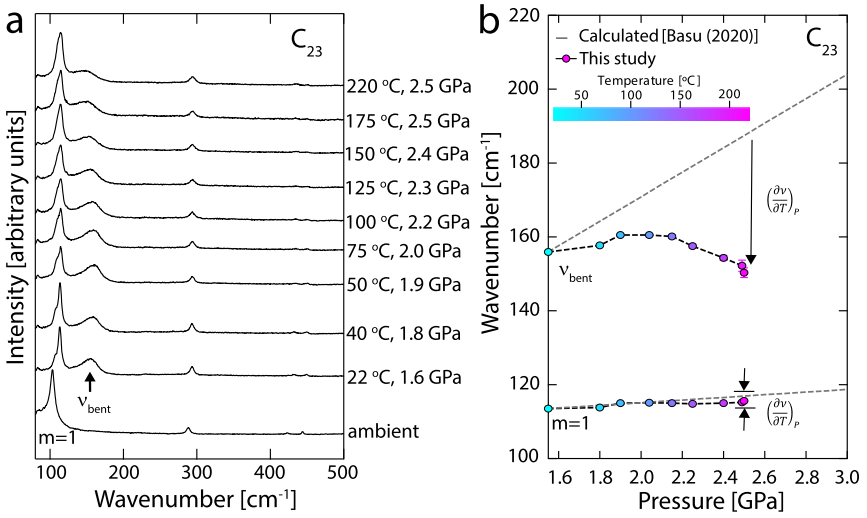

Figure 4. (a) Stacked Raman spectra of C_{23} in the low-energy region between 100 and 500 cm^{-1}. The temperature, applied through resistive heating in an HDAC, is shown along with the observed pressures. The fundamental LAM (m = 1) and the new bent mode (ν_{bent}) are indicated. (b) Plot of the fundamental LAM (m = 1) and ν_{bent} mode of C_{23} as a function of pressure is shown. The temperature is shown as a color contour. The color scale is shown in the inset, as a reference, with cyan color indicative of lower temperatures and magenta indicative of higher temperatures. The dashed line represents the pressure dependence of the ν_{bent} mode at room-temperature compression, where the $(\partial\nu/\partial P)_{22\ °C}$ is obtained from previous estimates,[25] and ν_0 is obtained from this study. The $(\partial\nu/\partial T)_P$ indicates the difference in the mode frequency between the static room temperature[25] and the HDAC high temperature (this study) measurements at a constant pressure. Please refer to the result section which elaborates further.

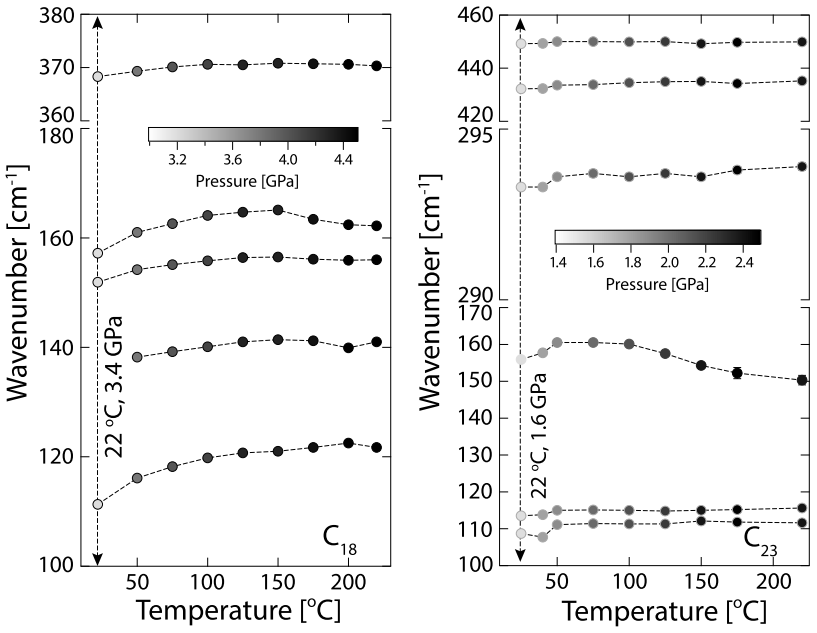

Figure 5. Temperature dependence of the low wavenumber modes of C_{18} and C_{23}. The thermal pressure due to heating of the sample in the HDAC is shown with a gray color contour scale. The light gray color indicates relatively low pressure, while the dark gray color represents higher pressure.

transition pressure, P_{tr}.[25,26] These recent studies showed that the transition pressure, P_{tr}, varied inversely with the chain length of alkane, that is, longer alkanes transformed from linear to bent configurations at lower pressures than the relatively shorter alkanes. The transition was always accompanied by the appearance of new low-energy modes in both high-pressure experiments and complementary *first-principles* simulations. Therefore, to explore the behavior of the bent alkane chains at moderate pressure and temperature, we initially compressed the C_{18} and C_{23} (in separate runs) to the transition pressure at room temperature and then externally heated it using resistive HDAC up to ∼220 °C. On initial room temperature compression of the alkane samples to the transition pressure, we notice the appearance of the new mode (ν_{bent}) related to the transformation of the linear chain to its bent configuration. For C_{18}, we observed the mode at ∼3.0 GPa, while for C_{23}, the mode appeared at ∼1 GPa (Figures 3 and 4). The two observations are in agreement with previous room-temperature compression measurements.[25,26] Once the appearance of the new mode was confirmed due to the bent chain configuration, we heated the samples in small increments to 220 °C and simultaneously collected the Raman spectra in the wave-

https://doi.org/10.1021/acs.jpcb.1c10786
J. Phys. Chem. B 2022, 126, 2530−2537

Table 1. Temperature Deviation of the Modes of Octadecane[a]

mode	$\nu_{Pmax,T}$[cm^{-1}]	$\sigma(\nu_{P_{max},T})$	$(\partial\nu/\partial T)_{Pmax}$ [cm^{-1}/°C]	$\sigma\ (\partial\nu/\partial T)_{Pmax}$	$(\partial\nu/\partial P)_{22\ °C}$ [cm^{-1}/GPa]	$\sigma\ (\partial\nu/\partial P)_{22\ °C}$
LAM; m = 1	156.0	0.1	−0.009	0.016	5.3	0.1
ν_{bent}	162.2	0.2	−0.041	0.256	11.8	3.5
LAM; m = 3	370.3	0.2	−0.013	0.047	4.1	0.1
H−C−H rock	902.2	0.3	−0.005	0.382	3.6	0.3
C−C symmetric stretch	1031.6	1.4	−0.011	0.194	5.6	0.2
C−C symmetric stretch	1058.7	0.4	−0.017	0.119	4.6	0.1
C−C asymmetric stretch	1074.7	0.0	−0.009	0.572	3.8	0.4
C−C stretch	1100.4	0.3	−0.012	0.486	4.6	0.4
H−C−H bend	1470.5	0.1	−0.012	0.136	5.5	0.1
CH_3 symmetric stretch	2915.8	0.1	−0.035	0.555	13.3	0.5
CH_3 asymmetric stretch	3002.7	0.4	−0.024	0.227	13.5	0.2

[a]Note: The $\nu_{Pmax,T}$ are the mode frequency observed in this study at the maximum pressure, P_{max} = 4.5 GPa (T = 220 °C). The temperature deviation of the modes is indicated by $(\partial\nu/\partial T)_{Pmax}$. The room-temperature pressure dependence[26] is indicated by $(\partial\nu/\partial P)_{22\ °C}$.

Table 2. Temperature Deviation of the Modes of Tricosane[a]

mode	$\nu_{Pmax,T}$ [cm^{-1}]	$\sigma(\nu_{Pmax,T})$	$(\partial\nu/\partial T)_{Pmax}$ [cm^{-1}/°C]	$\sigma\ (\partial\nu/\partial T)_{Pmax}$	$(\partial\nu/\partial P)_{22\ °C}$ [cm^{-1}/GPa]	$\sigma(\partial\nu/\partial P)_{22\ °C}$
LAM; m = 1	115.6	0.1	−0.007	0.033	3.6	0.2
ν_{bent}	150.3	1.3	−0.188	0.047	33.2	1.4
LAM; m = 3	293.9	0.1	−0.014	0.086	3.5	0.2
ω_3	449.9	1.0	−0.008	0.100	2.4	0.1
H−C−H rock	895.5	0.1	−0.009	0.303	3.0	0.2
C−C symmetric stretch	1064.1	0.1	−0.020	0.251	4.3	0.2
C−C symmetric stretch	1070.4	0.2	−0.026	0.264	6.2	0.3
C−C asymmetric stretch	1135.9	0.1	−0.033	0.394	4.4	0.3
H−C−H bend	1453.3	0.5	−0.016	0.462	3.2	0.2
CH_3−CH_2 stretch	2729.5	0.3	−0.024	0.262	5.3	0.1
CH_2 asymmetric stretch	2882.9	0.2	0.004	0.550	5.3	0.2
ω_5 Fermi resonance	2904.4	0.1	0.006	0.213	6.9	0.1
CH_3 symmetric stretch	2931.3	0.4	−0.011	0.451	6.6	0.2

[a]Note: The $\nu_{Pmax,T}$ are the mode frequency observed in this study at the maximum pressure, P_{max} = 2.5 GPa (T = 220 °C). The temperature deviation of the modes is indicated by $(\partial\nu/\partial T)_{Pmax}$. The room-temperature pressure dependence[25] is indicated by $(\partial\nu/\partial P)_{22\ °C}$.

number region from 100 to 3000 cm^{-1} at each temperature step. Due to the unique setup of the HDAC, we observe an increase in pressure with each temperature step. We corrected the temperature-induced shifts of the ruby line using a previous report.[33]

On deconvolution of the Raman spectra of C_{18} at 3.4 GPa and 22 °C, we find four prominent modes in the wavenumber region 100−600 cm^{-1}. The fundamental LAM was observed at 151.9 cm^{-1}, and ν_{bent} was observed as a high-energy shoulder to fundamental LAM at 157.2 cm^{-1}. On increasing the temperature to 50 °C, we observed another low-energy mode below the fundamental LAM at 138.2 cm^{-1}. Further increase in temperature resulted in a broad stiffening of most of the modes except for ν_{bent}, which shows softening around ∼100−150 °C (Figure 5). Similarly, for C_{23}, on deconvolution of the Raman spectra at 1.6 GPa and 22 °C, we observe six modes in the wavenumber region from 100 to 600 cm^{-1}. The fundamental LAM was observed at 113.8 cm^{-1}, and ν_{bent} was observed at 157.7 cm^{-1} (Figure 4). On heating, we observe all the modes, except the ν_{bent}, to stiffen and demonstrate a linear relationship between the mode frequency and temperature. The ν_{bent} mode for C_{23} reveals an inflection point at ∼50 to 100 °C, earlier than that observed in C_{18} (Figure 5). The higher energy mode frequencies of C_{18} and C_{23} stiffens on heating to 220 °C, and we do not observe any drastic changes in the spectral features indicative of phase transition (Supporting Information).

4. DISCUSSION

4.1. Compressional Behavior of C_{18} and C_{23}. Previous studies have indicated that a single chain of alkane, when suspended in a vacuum at low temperatures, exists in a linear extended conformation.[34,35] As the chain length increases to n ∼ 17−18, the weak interaction between segments of the chain introduces a hairpin bend in the alkane.[35] An alkane with a bent configuration is generally characterized by the appearance of new modes close to the fundamental LAM.[25,26,35] Furthermore, the fundamental LAM frequency of alkane chains is approximately inversely proportional to the chain length, n, which indicates that the new modes are modified LAM frequency due to the formation of shorter chain segments (e.g., i and j are the length of chain segments such that $i + j = n$). The length of each segment (i.e., i and j) can vary as the bend may be introduced on compression at different points in the alkane chain. Indeed, in a previous study, several bent configurations for tricosane were considered, and the effects of the length of the chain segment on the frequency of the bent mode were explored.[25] It was revealed that all the bent configurations generated the bent modes albeit at different frequencies depending on the length of each chain segment. Additionally, the bending of the alkane chains under compression can be accompanied by changes in orientational ordering. Recently, Puerto and Balzaretti[36] reported a conformational transition under compression in C_{23} around 2−5 GPa.

https://doi.org/10.1021/acs.jpcb.1c10786
J. Phys. Chem. B 2022, 126, 2530−2537

4.2. High-Pressure and High-Temperature Behavior of C_{18} and C_{23}. In the present study, on heating C_{18} and C_{23} to 220 °C in an HDAC, we observe two successive events where the ν_{bent} mode frequency initially stiffens followed by a softening. We suspect that the interplay of heating and compression (due to the thermal pressure) results in the occurrence of these two events. To decouple the effects of the simultaneous heating and compression, it will be important to understand the deviation in the behavior of the ν_{bent} mode due to the thermal pressure from the room-temperature compression.

The pressure and temperature dependence of vibrational mode frequencies ($\nu_{P,T}$) could be quantified via the formalism

$$\nu_{P,T} = \nu_0 + \left(\frac{\partial \nu}{\partial P}\right)_T dP + \left(\frac{\partial \nu}{\partial T}\right)_P dT$$

where ν_0 refers to the vibrational mode at 1 bar and 22 °C, $(\partial\nu/\partial P)_T$ refers to the pressure dependence of the vibrational modes at a constant temperature, and $(\partial\nu/\partial T)_P$ refers to the temperature dependence of the vibrational modes at a constant pressure. Often, static compression studies provide constraints on $(\partial\nu/\partial P)_T$ (T = 22 °C). Similarly, high-temperature studies often provide constraints on $(\partial\nu/\partial T)_P$, ($P$ = 1 bar). Indeed, recent studies on two alkanes (C_{18} and C_{23}) provided valuable constraints on $(\partial\nu/\partial P)_{22\ °C}$ (Tables 1 and 2).[25,26] In this present study, we aim to understand the behavior of the ν_{bent} mode, which is not present at ambient pressures and thus pose a challenge as we are unable to constrain $(\partial\nu/\partial T)_{1\ bar}$. However, we are able to provide constraints on $(\partial\nu/\partial T)_{P_{max}}$, where P_{max} is the maximum thermal pressure explored in our study using the formalism

$$\left(\frac{\partial \nu}{\partial T}\right)_{P_{max}} = \frac{\nu_{P_{max},T} - \nu_{P_{max},22\ °C}}{T - 22\ °C}$$

where $\nu_{Pmax,22\ °C} = \nu_{P,22\ °C} + (\partial\nu/\partial P)_{22\ °C}(P_{max} - 1\ bar)$.

We note that for octadecane, most of the modes at the low-energy region (100−1200 cm^{-1}) show a $(\partial\nu/\partial T)_{Pmax}$ that ranges from −0.005 (±0.382) to −0.017 (±0.119) $cm^{-1}/°C$ with notable exception displayed by the ν_{bent} mode, which exhibits $(\partial\nu/\partial T)_{Pmax}$∼−0.041 (±0.256) $cm^{-1}/°C$ (Table 1). In comparison to the tricosane low-energy region (100−1200 cm^{-1}), the effect of temperature on the ν_{bent} mode is even more pronounced with $(\partial\nu/\partial T)_{Pmax}$ ∼ −0.188 (±0.047) $cm^{-1}/°C$ (Table 2). We also note that the vibrational modes that are most sensitive to pressures with greater $(\partial\nu/\partial P)_{22\ °C}$ are the ones that also have large $(\partial\nu/\partial T)_{Pmax}$. When we compare the ν_{bent} mode with the LAM (m = 1) mode that is closest in energy, we find that $(\partial\nu/\partial T)_{Pmax}$ for the ν_{bent} mode is 10−100 times greater than that of LAM (m = 1) mode (Figures 3b and 4b). It is very likely that $(\partial\nu/\partial T)_{Pmax}$ for the LAM (m = 1) is due to anharmonic effects; in contrast, it is likely that the $(\partial\nu/\partial T)_{Pmax}$ for the ν_{bent} mode has contributions from both "anharmonicity" and "unbending," that is, $\left(\frac{\partial \nu}{\partial T}\right)_{P_{max}} = \left(\frac{\partial \nu}{\partial T}\right)^{anharmonic}_{P_{max}} + \left(\frac{\partial \nu}{\partial T}\right)^{unbending}_{P_{max}}$. The modes that are not associated with the bending of the alkane chains are likely to have $\left(\frac{\partial \nu}{\partial T}\right)^{unbending}_{P_{max}} = 0$. We note that at the maximum pressure and temperature conditions explored in our study, the ν_{bent} mode persists, which indicates that the large-chain alkanes are still in a bent configuration but likely to have undergone some amount of unbending due to heating. If this is true, further higher temperatures are required for complete unbending. This, however, often induces thermal pressure, which may lead to bending. Thus, overall the opposing effects of pressure and temperatures will ultimately dictate the "bent" or "unbent" state of large alkanes. Since our goal was to elucidate the stability of these hydrocarbons in the interiors of meteorites during entry and passage through the Earth's atmosphere, we explored pressures and temperatures that are likely to be relevant for such an event, while a temperature higher than 220 °C is outside our current interest.

A major factor for the survival and delivery of hydrocarbons is the temperature experienced during the atmospheric entry and passage of the IDPs, MMs, and meteorites. The peak surface temperature reached during entry into the Earth's atmosphere is in the range of 400−1700 °C.[12−15,18] The majority of aromatic and aliphatic hydrocarbons have low thermal stability. The aromatic hydrocarbons coronene[37] and benzene[38] have been observed to dissociate into elemental C and H_2 around 400−600 °C, while similar dissociation of methane[39] was observed around 700−1000 °C (Figure 6).

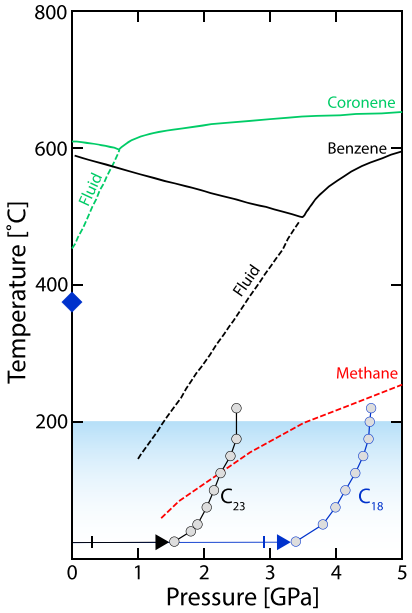

Figure 6. Pressure and temperature region explored in this study. The arrow shows the initial compression path at room temperature (black: C_{23} and blue: C_{18}). The vertical black (blue) line indicates the transformation of C_{23} (C_{18}) from a linear chain to the bent configuration. The solid gray circles indicate the heating path. The dashed line indicates the melting boundary, and the solid line indicates the dissociation boundary (green: coronene;[37] black: benzene;[38] and red: methane[39]). The blue diamond is the dissociation point of octadecane to shorter chains at 375 °C when heated for 73 h at ambient pressure.[40] The blue shaded region indicates the peak temperature experienced in the interior of meteorites during atmospheric passage.[19]

Temperature-dependent studies (up to ∼375 °C) on C_{18}, conducted at ambient pressures, noted partial dissociation to methane, ethane, propane, and butane.[40] In a preliminary laser-heated measurement to >2000 °C on C_{18}, we find the appearance of new modes in the H−C−H bending region, likely indicating the formation of different species of hydrocarbon (Supporting Information). However, an extensive

https://doi.org/10.1021/acs.jpcb.1c10786
J. Phys. Chem. B 2022, 126, 2530−2537

mapping of pressures and temperatures is warranted for a thorough understanding of the transformation and/or dissociation mechanism of the alkanes at elevated $P-T$ conditions for the laser-heated measurements. In the present study, while a single $P-T$ path was probed for each alkane sample in the HDAC experiments, we do not observe any indication of dissociation of C_{18} and C_{23} to the highest $P-T$ values.

Although the survivability of aliphatic hydrocarbons during entry into the atmosphere is unlikely due to their low thermal stability and high peak surface temperature experienced, their abundance in several extraterrestrial objects is paradoxical. The substantial temperature gradient and the kinetic effects associated with the transformation processes in the incoming extraterrestrial matter were proposed as a possible explanation for the survivability of the organic matter.[12,14,19] Indeed, the phase stability of C_{18} and C_{23} across the pressure−temperature range, explored in the HDAC measurements corresponding to the temperature experienced in the interiors of the extraterrestrial objects, supports the scenario of temperature gradient effects (Figure 6).

5. CONCLUSIONS

To summarize, we have investigated the behavior of aliphatic hydrocarbons at temperatures up to 220 °C. The HDAC measurements on C_{18} and C_{23} reactivity reveal that, at moderate $P-T$ conditions relevant for the interior of extraterrestrial objects, the alkanes are mostly stable and do not show any dissociation. The initial compression of the alkanes at room temperature results in the appearance of a new mode, ν_{bent}, related to the bending of the linear alkane chains. On heating, we observe the ν_{bent} mode to stiffen initially and then undergo a softening. Such softening of the ν_{bent} mode on heating can be explained by considering an unbending of the bent alkane chain and mode anharmonicity. This newly documented temperature response of alkane chains should be taken into account in the survivability of the hydrocarbons in extraterrestrial objects.

■ ASSOCIATED CONTENT

Supporting Information

The Supporting Information is available free of charge at https://pubs.acs.org/doi/10.1021/acs.jpcb.1c10786.

> Stacked Raman spectra of octadecane in the wavenumber region 800−3200 cm^{-1}; stacked Raman spectra of tricosane in the wavenumber region 800−3200 cm^{-1}; and preliminary laser-heated spectra of octadecane (PDF)

■ AUTHOR INFORMATION

Corresponding Author

Abhisek Basu − *Earth Materials Laboratory, Department of Earth, Ocean and Atmospheric Science, Florida State University, Tallahassee, Florida 32306, United States;* orcid.org/0000-0002-0283-1778; Email: abasu@fsu.edu

Authors

Mainak Mookherjee − *Earth Materials Laboratory, Department of Earth, Ocean and Atmospheric Science, Florida State University, Tallahassee, Florida 32306, United States;* orcid.org/0000-0002-0605-5964

Ericka McMahan − *Earth Materials Laboratory, Department of Earth, Ocean and Atmospheric Science, Florida State University, Tallahassee, Florida 32306, United States*

Bianca Haberl − *Neutron Scattering Division, Neutron Sciences Directorate, Oak Ridge National Laboratory, Oak Ridge, Tennessee 37831, United States;* orcid.org/0000-0002-7391-6031

Reinhard Boehler − *Neutron Scattering Division, Neutron Sciences Directorate, Oak Ridge National Laboratory, Oak Ridge, Tennessee 37831, United States*

Complete contact information is available at: https://pubs.acs.org/10.1021/acs.jpcb.1c10786

Notes

The authors declare no competing financial interest.

■ ACKNOWLEDGMENTS

This work is funded by the National Science Foundation (NSF) (EAR 1753125, 1638752, and 1248553). A.B. acknowledges the Dean's Teaching Postdoctoral Fellowship from the College of Arts and Sciences, Florida State University. B.H. and R.B. were supported by resources at the Spallation Neutron Source and the High Flux Isotope Reactor, DOE Office of Science User Facilities operated by the Oak Ridge National Laboratory (ORNL).

■ REFERENCES

(1) Dodd, R. T. *Meteorites: A Chemical and Petrological Synthesis*; Cambridge University Press: Cambridge, 1981.

(2) Sephton, M. A. Organic Compounds in Carbonaceous Meteorites. *Nat. Prod. Rep.* **2002**, *19*, 292−311. The Royal Society of Chemistry May

(3) Martins, Z. Organic Molecules in Meteorites. *Proc. Int. Astron. Union* **2015**, *11*, 411−415.

(4) Martins, Z.; Modica, P.; Zanda, B.; d'Hendecourt, L. L. S. The amino acid and hydrocarbon contents of the Paris meteorite: Insights into the most primitive CM chondrite. *Meteorit. Planet. Sci.* **2015**, *50*, 926−943.

(5) Sephton, M. A. Organic Geochemistry of Meteorites. *Treatise Geochem.* **2014**, *12*, 1−31 Elsevier.

(6) Pizzarello, S.; Cooper, G. W.; Flynn, G. J. The Nature and Distribution of the Organic Material in Carbonaceous Chondrites and Interplanetary Dust Particles. In *Meteorites and the Early Solar System II*; Lauretta, D. S., McSweenJr, H. Y., Eds.; University of Arizona Press: Tucson, 2006, pp 625−652.

(7) Glavin, D. P.; Alexander, C. M. O. D.; Aponte, J. C.; Dworkin, J. P.; Elsila, J. E.; Yabuta, H. The Origin and Evolution of Organic Matter in Carbonaceous Chondrites and Links to Their Parent Bodies. In *Primitive Meteorites and Asteroids*; Elsevier, 2018, pp 205−271. DOI: 10.1016/B978-0-12-813325-5.00003-3.

(8) Flynn, G. J.; Keller, L. P.; Jacobsen, C.; Wirick, S. Carbon Mapping and Carbon-XANES Bonding State Measurements on

Interplanetary Dust Particles. In *Lunar and Planetary Science Conference*; 1998; p 1159.
(9) Flynn, G. J.; Keller, L. P.; Miller, M. A. FTIR Detection of Organic Carbon in Interplanetary Dust Particles. In *Lunar and Planetary Science Conference*; 1998; p 1157.
(10) Flynn, G. J.; Keller, L. P.; Feser, M.; Wirick, S.; Jacobsen, C. The Origin of Organic Matter in the Solar System: Evidence from the Interplanetary Dust Particles. *Geochim. Cosmochim. Acta* **2003**, *67*, 4791−4806.
(11) Keller, L. P.; Messenger, S.; Flynn, G. J.; Clemett, S.; Wirick, S.; Jacobsen, C. The Nature of Molecular Cloud Material in Interplanetary Dust. *Geochim. Cosmochim. Acta* **2004**, *68*, 2577−2589.
(12) Matrajt, G.; Brownlee, D.; Sadilek, M.; Kruse, L. Survival of Organic Phases in Porous IDPs during Atmospheric Entry: A Pulse-Heating Study. *Meteorit. Planet. Sci.* **2006**, *41*, 903−911.
(13) Flynn, G. J. Atmospheric Entry Heating: A Criterion to Distinguish between Asteroidal and Cometary Sources of Interplanetary Dust. *Icarus* **1989**, *77*, 287−310.
(14) Love, S.; Brownlee, D. E. Heating and thermal transformation of micrometeoroids entering the Earth's atmosphere. *Icarus* **1991**, *89*, 26−43.
(15) Brownlee, D. E.; Joswiak, D. J.; Love, S. G.; Bradley, J. P. Identification of Cometary and Asteroidal Particles in Stratospheric Idp Collections. In *24th Lunar and Planetary Science Conference*, 1993, pp 205−206.
(16) Joswiak, D. J.; Brownlee, D. E.; Pepin, R. O.; Schlutter, D. J. Mineralogy and Densities of Cometary and Asteroidal IDPs Collected in the Stratosphere. In *Dust in Planetary Systems*; 2005; Vol. 1280, p 85.
(17) Joswiak, D. J.; Brownlee, D. E.; Pepin, R. O.; Schlutter, D. J. Characteristics of Asteroidal and Cometary IDPs Obtained from Stratospheric Collectors: Summary of Measured He Release Temperatures, Velocities and Descriptive Mineralogy. In *Lunar and Planetary Science Conference*; 2000; p 1500.
(18) Sandford, S. A.; Bradley, J. P. Interplanetary Dust Particles Collected in the Stratosphere: Observations of Atmospheric Heating and Constraints on Their Interrelationship and Sources. *Icarus* **1989**, *82*, 146−166.
(19) Sears, D. W. Temperature Gradients in Meteorites Produced by Heating during Atmospheric Passage. *Mod. Geol.* **1975**, *5*, 155−164.
(20) Svec, H. J.; Clyde, D. D. Vapor Pressures of Some α-Amino Acids. *J. Chem. Eng. Data* **1965**, *10*, 151−152.
(21) Mango, F. D. The stability of hydrocarbons under the time-temperature conditions of petroleum genesis. *Nature* **1991**, *352*, 146−148.
(22) Price, L. C.; Clayton, J. L.; Rumen, L. L. Organic Geochemistry of the 9.6 Km Bertha Rogers No. 1. Well, Oklahoma. *Org. Geochem.* **1981**, *3*, 59−77.
(23) Hayes, J. M. Stability of Petroleum. *Nature* **1991**, *352*, 108−109.
(24) Zerr, A.; Serghiou, G.; Boehler, R.; Ross, M. Decomposition of Alkanes at High Pressures and Temperatures. *High Pressure Res.* **2006**, *26*, 23−32.
(25) Basu, A.; Murphy, P.; Mookherjee, M.; Haberl, B.; Boehler, R. High-Pressure Behavior of a Linear Chain Alkane, Tricosane. *J. Appl. Phys.* **2020**, *127*, 105901.
(26) Basu, A.; Mookherjee, M.; Schiffert, C.; Haberl, B.; Boehler, R. Spectroscopic Investigation of the High-Pressure Behavior of Aliphatic Hydrocarbon: Implications for Planetary Processes. *ACS Earth Space Chem.* **2021**, *5*, 449−456.
(27) Basu, A.; Mookherjee, M. Intercalation of Water in Kaolinite ($Al_2Si_2O_5(OH)_4$) at Subduction Zone Conditions: Insights from Raman Spectroscopy. *ACS Earth Space Chem.* **2021**, *5*, 834−848.
(28) Bassett, W. A.; Shen, A. H.; Bucknum, M.; Chou, I. M. A new diamond anvil cell for hydrothermal studies to 2.5 GPa and from −190 to 1200 °C. *Rev. Sci. Instrum.* **1993**, *64*, 2340−2345.
(29) Bassett, W. A. High Pressure-Temperature Aqueous Systems in the Hydrothermal Diamond Anvil Cell (HDAC). *Eur. J. Mineral.* **2003**, *15*, 773−780.
(30) Luning Prak, D. J.; Lee, B. G.; Cowart, J. S.; Trulove, P. C. Density, Viscosity, Speed of Sound, Bulk Modulus, Surface Tension, and Flash Point of Binary Mixtures of Butylbenzene + Linear Alkanes (n-Decane, n-Dodecane, n-Tetradecane, n-Hexadecane, or n-Heptadecane) at 0.1 MPa. *J. Chem. Eng. Data* **2017**, *62*, 169−187.
(31) Mao, H. K.; Xu, J.; Bell, P. M. Calibration of the Ruby Pressure Gauge to 800 Kbar under Quasi-Hydrostatic Conditions. *J. Geophys. Res.* **1986**, *91*, 4673.
(32) Vandenabeele, P. *Practical Raman Spectroscopy: An Introduction*; John Wiley & Sons, 2013.
(33) Rekhi, S.; Dubrovinsky, L.; Saxena, S. Temperature-Induced Ruby Fluorescence Shifts up to a Pressure of 15 GPa in an Externally Heated Diamond Anvil Cell. *High Temp. - High Pressures* **1999**, *31*, 299−305.
(34) Byrd, J. N.; Bartlett, R. J.; Montgomery, J. A. At What Chain Length Do Unbranched Alkanes Prefer Folded Conformations? *J. Phys. Chem. A* **2014**, *118*, 1706−1712.
(35) Lüttschwager, N. O. B.; Wassermann, T. N.; Mata, R. A.; Suhm, M. A. The Last Globally Stable Extended Alkane. *Angew. Chem., Int. Ed.* **2013**, *52*, 463−466.
(36) Puerto, M. A.; Balzaretti, N. M. Raman and Infrared Vibrational Modes of Tricosane Paraffin under High Pressure. *Vib. Spectrosc.* **2014**, *75*, 93−100.
(37) Chanyshev, A. D.; Litasov, K. D.; Shatskiy, A. F.; Sharygin, I. S.; Higo, Y.; Ohtani, E. Transition from Melting to Carbonization of Naphthalene, Anthracene, Pyrene and Coronene at High Pressure. *Phys. Earth Planet. Inter.* **2017**, *270*, 29−39.
(38) Chanyshev, A. D.; Litasov, K. D.; Rashchenko, S. V.; Sano-Furukawa, A.; Kagi, H.; Hattori, T.; Shatskiy, A. F.; Dymshits, A. M.; Sharygin, I. S.; Higo, Y. High-Pressure-High-Temperature Study of Benzene: Refined Crystal Structure and New Phase Diagram up to 8 GPa and 923 K. *Cryst. Growth Des.* **2018**, *18*, 3016−3026.
(39) Lobanov, S. S.; Chen, P.-N.; Chen, X.-J.; Zha, C.-S.; Litasov, K. D.; Mao, H.-K.; Goncharov, A. F. Carbon Precipitation from Heavy Hydrocarbon Fluid in Deep Planetary Interiors. *Nat. Commun.* **2013**, *4*, 2446.
(40) Wang, X.; Song, Y.; Chou, I.-M.; Qiu, Y. Raman Spectroscopic Characterization of Cracking and Hydrolysis of n -Pentane and n -Octadecane at 300−375°C with Geological Implications. *Energy Explor. Exploit.* **2018**, *36*, 955−970.

https://doi.org/10.1021/acs.jpcb.1c10786
J. Phys. Chem. B 2022, 126, 2530−2537